

Analysis and Design of A High-Efficiency 6.78-MHz Wireless Power Transfer System with Scalable Number of Receivers

Jibin Song, *Student Member, IEEE*, Ming Liu, *Member, IEEE*, Chengbin Ma, *Senior Member, IEEE*

Abstract—For multiple-receiver wireless power transfer (WPT), a scalable solution is desired that functions with changing number of receivers. Meanwhile, challenges lie in differences in load characteristics, power level, and cross coupling between the receivers. This paper employs Class E² dc-dc converter topology for the multiple-receiver WPT systems working at megahertz (MHz). The shunt capacitor capacitances of the Class E rectifiers and magnitude of constant output current of the current-mode Class E power amplifier are chosen as design parameters aiming at decoupling the received power of each receiver. Design procedures are developed to simultaneously achieve high efficiency and desired individual load powers over a target variation range of the cross coupling. An experimental 6.78-MHz three-receiver WPT system is optimally designed. The system is shown to be capable of providing different target load powers (10, 8, 6 W) and maintaining a high system efficiency (above 70%) with different combinations and positions of the receivers.

Index Terms—Cross coupling, efficiency, load power distribution, multiple-receiver wireless power transfer (WPT), scalability.

I. INTRODUCTION

Megahertz (MHz) wireless power transfer (WPT) is now being considered as a promising candidate technology for the mid-range transfer of a medium amount of power. It is largely because a higher operating frequency such as 6.78 MHz helps to improve the spatial freedom of the power transfer, and also enables more compact and lighter WPT systems. Especially, MHz WPT makes it possible to charge multiple receivers with a single transmitting coil, namely multiple-receiver WPT systems. The conventional single-receiver WPT systems have been intensively investigated in recent years such as on power amplifiers (PAs) [1], rectifiers [2], and system-level design and control [3], [4]. The less-common multiple-receiver WPT systems also attracted interests. For example, multiple operating

frequencies, mostly for systems working at kilohertz, were applied to simultaneously transfer power to multiple receivers with different resonant frequencies, and thus meet respective power demand of each receiver. The circuit topology of the multiple-frequency power source will become complicated with an increasing number of receivers [5], [6]. In addition, the narrow industrial-scientific-medical (ISM) band imposes limitation on choosing the available operating frequencies [7]. Time division schemes were proposed that naturally avoid the influence of cross coupling among receivers [8], [9]. Since only one receiver is powered at one time, this approach simplifies the operation of a multiple-receiver WPT system, but compromises the duration to transfer a preferred amount of energy. Additional communication and control efforts are also required for its implementation. Placement of different number of receivers was designed to achieve identical load power for each receiver and maintain the same optimal operating frequency [10]. In both analysis and experiments, load resistances being connected to receiving coils were assumed to be identical. A game theory-based strategy was developed to actively control the power distribution among the receivers. Its implementation requires dedicated dc-dc converters and communication between the transmitting and receiving sides [11].

As mentioned above, for MHz WPT it is challenging to adjust the resonance frequency due to the narrow ISM band. Usually a fixed frequency, again such as 6.78 MHz, is preferred. Note that the 6.78 MHz is the lowest frequency in the globally accepted ISM (industrial, scientific, and medical) bands. It is the only frequency currently recommended by ITU-R (International Telecommunication Union Radiocommunication Sector) for consumer device wireless power transfer thanks to its minimal or non-existent impact to other licensed bands [7]. For a higher operating frequency at the ISM bands, such as 13.56 MHz or 27.12 MHz, it further improves spatial freedom, but increases switching loss and driving loss, and presents additional challenges for circuit design (e.g., PCB layout and components selection) and coupling coil design (e.g., low self-resistance). During the operation of multiple-receiver WPT systems, the uncertainties are mostly from the changing number of receivers, and their different sizes, positions, power requirements, and load characteristics. The interactions between the receivers, i.e., the cross coupling, also significantly influence the overall performance [12]. Thus a design methodology is particularly needed to achieve a multiple-receiver WPT system operating in such a dynamic environment, i.e., with a scalable number of receivers. This

© 2019 IEEE. Personal use of this material is permitted. Permission from IEEE must be obtained for all other uses, including reprinting/republishing this material for advertising or promotional purposes, collecting new collected works for resale or redistribution to servers or lists, or reuse of any copyrighted component of this work in other works.

Manuscript received Apr. 3, 2019; revised Jul. 5, 2019 and Sep. 16, 2019; accepted Oct. 13, 2019. This work was supported by the Shanghai Natural Science Foundation under Grant 16ZR1416300. (Corresponding author: Ming Liu.)

J. Song and C. Ma are with the University of Michigan-Shanghai Jiao Tong University Joint Institute, Shanghai Jiao Tong University, Shanghai 200240, China (e-mail: jibinsong@sjtu.edu.cn; chbma@sjtu.edu.cn).

M. Liu is with Department of Electrical Engineering, Princeton University, Princeton, NJ 08544, USA (e-mail: ml45@princeton.edu).

scalable solution should be capable to always provide the desired specific load power of each receiver when other receivers join or quit the charging, while at the same time maintain a high system efficiency. Targeting on real applications, the solution is expected to be as concise as possible, especially in circuit configuration. This requires proper selection of circuit topology and corresponding parameter design. The final solution should not only meet requirements at the nominal condition but also maintain a stable performance (e.g., efficiency and distributed load powers) when the uncertainties occur such as changing number of receivers and cross coupling.

Based on the above considerations, this paper proposes a systematic circuit design methodology to realize multiple-receiver MHz systems that operate with a scalable number of receivers. This design methodology is particularly useful for the applications where the receivers have different load characteristics, different power levels, and changing relative positions in a common wireless charging area (e.g., smartphones, smartwatches, and earbuds). A Class E^2 dc-dc converter topology (i.e., with both Class E PA and Class E rectifiers) is selected due to its high efficiency, namely the soft-switching property, when working at MHz. Another purpose of choosing the Class E rectifiers is to provide a degree of freedom to design the rectifier input impedances, and thus adjust the received power in individual receivers and improve system efficiency, via properly selected shunt capacitor capacitances of these rectifiers. The output current of a modified current-mode Class E PA and shunt capacitor capacitances of the respective Class E rectifiers in the receivers are particularly chosen as design parameters. They are optimally designed to maintain desired load power of each receiver and high efficiency at the same time. The influences of the cross coupling are analyzed and reflected in the design optimization problem, which is formulated to take the variations in number of receivers and cross coupling into account. The proposed solution takes unique advantages of the Class E^2 topology, especially its high efficiency at MHz and possibility to design the rectifier input impedances through choosing different shunt capacitor capacitances of the Class E rectifiers. This solution enables a high efficiency multiple-receiver WPT system with a scalable number of receivers, i.e., decoupled load power distribution. Besides, its implementation does not need complicated circuits and control schemes mentioned in the above existing works [5], [6], [8]–[11]. Both the following theoretical analysis and design methodology add new insights into the development of efficient and robust multiple-receiver WPT systems that work in dynamic environments.

II. DERIVATIONS AND ANALYSIS

A. Power Distribution Mechanism

Fig. 1 shows the proposed Class E^2 multiple-receiver WPT system working at 6.78 MHz. It consists of one transmitter TX and n receivers RX_i ($i = 1, \dots, n$). For the scalability of the multi-receiver system, a Π impedance transformation network (L_{mn} , C_{ml} , and C_{mr}) is added after the classical Class E PA to form a current-mode (CM) Class E PA. Note that in the following discussions, the CM Class E PA refers

to the combination of the classical Class E PA and the Π impedance transformation network, as shown in the circuit model of the transmitter in Fig. 1(a). This PA is designed later in Section III-B to provide an almost constant output current over a wide range of loading conditions. Unlike the finite inductor of the resonant Class E rectifier in [13], $L_{f,i}$ of the i -th rectifier in this paper is an infinite RF choke inductor that provides a dc current path for the rectifier output current [3]. The rectifier works like a Class E PA with an infinite RF choke. The shunt capacitor $C_{r,i}$ shapes the diode voltage and turns the diode on and off at low dv/dt , reducing the switching loss and noise [14]. This paper proposes the design of the rectifier shunt capacitors, $C_{r,i}$'s, that tunes the powers received by individual receivers, and at the same time, maintains a high system efficiency. Note that here the diode parasitic capacitors are absorbed into their respective shunt capacitors. In general, the shunt capacitors are much larger than the diode parasitic capacitances. Thus, during circuit analysis, the variance of the diode parasitic capacitances is usually assumed to be negligible. In the figure, r_{tx} , $r_{rx,i}$, $r_{L_{f,i}}$, and $r_{D_{r,i}}$ are the equivalent resistances (ESRs) of the transmitting coil (C_{tx} and L_{tx}), receiving coils ($C_{rx,i}$ and $L_{rx,i}$), rectifier RF choke ($L_{f,i}$), and rectifying diodes $D_{r,i}$, respectively.

Fig. 1(b) gives the simplified equivalent circuit of the multiple-receiver WPT system, in which the CM Class E PA is represented as a constant current source (\mathbf{I}_{tx}) and the input impedance of the Class E rectifier is $R_{rec,i} + jX_{rec,i}$. Note that bold symbols in this paper denote complex quantities and vectors. k_{ti} is the mutual inductance coefficient describing the coupling between TX and RX_i ; k_{ij} is the mutual inductance coefficient representing the cross coupling between RX_i and RX_j .

The compensation capacitors, C_{tx} and $C_{rx,i}$, should be designed to make the coils, both the transmitting and receiving ones, fully resonant to improve power transfer capability and efficiency, i.e.,

$$j\omega L_{tx} + \frac{1}{j\omega C_{tx}} = 0, \quad (1)$$

$$j\omega L_{rx,i} + \frac{1}{j\omega C_{rx,i}} + jX_{rec,i} = 0, \quad (2)$$

where $X_{rec,i}$ is the input reactance of the i -th rectifier at the operating frequency, 6.78 MHz here, namely a non-pure-resistive input impedance of the rectifier [refer to (8)]. Applying the Kirchhoff's Voltage Law (KVL) gives the relationship between the input voltage (\mathbf{V}_{tx}) of TX and currents (\mathbf{I}_{tx} and $\mathbf{I}_{rx,i}$'s) of TX and RX_i , as shown in (3). M_{ti} and M_{ij} are the mutual inductances among the coupling coils,

$$M_{ti} = k_{ti} \sqrt{L_{tx} L_{rx,i}}, \quad (4)$$

$$M_{ij} = k_{ij} \sqrt{L_{rx,i} L_{rx,j}}. \quad (5)$$

From (3), the ratio of $\mathbf{I}_{rx,i}$ and \mathbf{I}_{tx} can then be solved as

$$\mathbf{R}_{tr,i} = \frac{\mathbf{I}_{rx,i}}{\mathbf{I}_{tx}}, \quad (6)$$

$$\frac{\mathbf{I}_{rx,1}}{\mathbf{I}_{tx}} = \frac{A}{B},$$

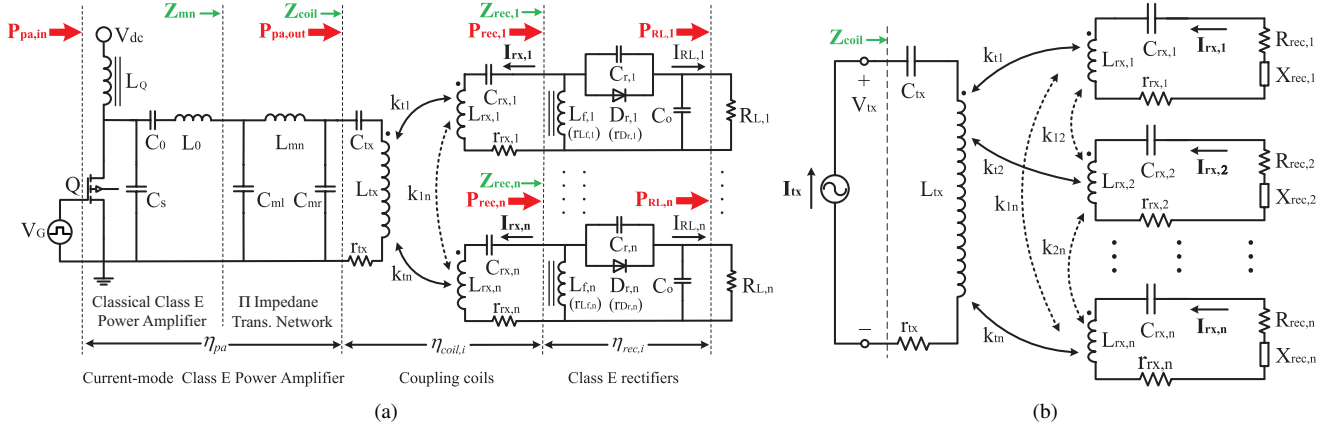


Fig. 1. Class E^2 multiple-receiver WPT system. (a) Circuit model. (b) Equivalent circuit.

$$\begin{bmatrix} \mathbf{V}_{tx} \\ 0 \\ 0 \\ \vdots \\ 0 \end{bmatrix} = \begin{bmatrix} r_{tx} & j\omega M_{t1} & j\omega M_{t2} & \cdots & j\omega M_{tn} \\ j\omega M_{t1} & r_{rx,1} + R_{rec,1} & j\omega M_{12} & \cdots & j\omega M_{1n} \\ j\omega M_{t2} & j\omega M_{12} & r_{rx,2} + R_{rec,2} & \cdots & j\omega M_{2n} \\ \vdots & \vdots & \vdots & \ddots & \vdots \\ j\omega M_{tn} & j\omega M_{1n} & j\omega M_{2n} & \cdots & r_{rx,n} + R_{rec,n} \end{bmatrix} \begin{bmatrix} \mathbf{I}_{tx} \\ \mathbf{I}_{rx,1} \\ \mathbf{I}_{rx,2} \\ \vdots \\ \mathbf{I}_{rx,n} \end{bmatrix}. \quad (3)$$

$$\begin{aligned} A &= jM_{12}M_{23}M_{t3}\omega^3 + jM_{13}M_{23}M_{t2}\omega^3 \\ &- jM_{23}^2M_{t1}\omega^3 - M_{12}M_{t2}(r_{rx,3} + R_{rec,3})\omega^2 \\ &- M_{13}M_{t3}(r_{rx,2} + R_{rec,2})\omega^2 \\ &- j\omega M_{t1}(r_{rx,2} + R_{rec,2})(r_{rx,3} + R_{rec,3}), \\ B &= (r_{rx,1} + R_{rec,1})(r_{rx,2} + R_{rec,2})(r_{rx,3} + R_{rec,3}) \\ &+ M_{12}^2(r_{rx,3} + R_{rec,3})\omega^2 \\ &+ M_{13}^2(r_{rx,2} + R_{rec,2})\omega^2 \\ &+ M_{23}^2(r_{rx,1} + R_{rec,1})\omega^2 \\ &- 2M_{12}M_{13}M_{23}\omega^3. \end{aligned} \quad (7)$$

As shown in (7) taking $\frac{\mathbf{I}_{rx,1}}{\mathbf{I}_{tx}}$ in a three-receiver WPT system as an example, $\mathbf{R}_{tr,i}$ is determined by M_{ti} and M_{ij} , ESRs of the receiving coils ($r_{rx,i}$'s), and input resistances of the rectifiers ($R_{rec,i}$'s). The input impedances of rectifiers, $\mathbf{Z}_{rec,i}$, (i.e., $R_{rec,i}$ too) can be derived as follows,

$$\begin{aligned} \mathbf{Z}_{rec,i} &= R_{rec,i} + jX_{rec,i}, \\ R_{rec,i} &= 2(R_{L,i} + r_{L_f,i})\sin^2\phi_{rec,i} + 2c_i r_{D_r,i}, \\ X_{rec,i} &= -\frac{1}{\pi} \left(\frac{e_i}{\omega C_{r,i}} + r_{D_r,i} f_i \right), \end{aligned} \quad (8)$$

where

$$\begin{aligned} c_i &= \frac{D_i}{2} + D_i \sin^2\phi_{rec,i} \\ &- \frac{1}{\pi} \sin\phi_{rec,i} \cos(\phi_{rec,i} - 2\pi D_i) \\ &+ \frac{1}{8\pi} \sin(2\phi_{rec,i} - 4\pi D_i) + \frac{3}{8\pi} \sin 2\phi_{rec,i}, \\ e_i &= \pi(1 - D_i)[1 + 2\sin\phi_{rec,i} \sin(\phi_{rec,i} - 2\pi D_i)] \\ &+ \frac{1}{4} [\sin(2\phi_{rec,i} - 4\pi D_i) - \sin(2\phi_{rec,i})] \\ &+ \sin(2\pi D_i), \end{aligned}$$

$$\begin{aligned} f_i &= \frac{1}{2} - \frac{\cos(2\phi_{rec,i})}{4} - \frac{\cos(2\phi_{rec,i} - 4\pi D_i)}{4} \\ &- \sin\phi_{rec,i} \sin(\phi_{rec,i} - 2\pi D_i). \end{aligned} \quad (9)$$

The intermediate variables, c_i , e_i and f_i , are the functions of $\phi_{rec,i}$ and D_i [3]. Here $\phi_{rec,i}$ and D_i are the initial phase of the sinusoidal input current of the i -th rectifier and the duty cycle of the rectifying diode $D_{r,i}$, respectively [15]. As shown in the below equations, (11)(12), $\phi_{rec,i}$ and D_i , as well as $X_{rec,i}$, relate to $R_{L,i}$. For the half-wave Class E rectifiers, their output currents can be determined as (i.e., the values when $\omega t = 0$)

$$I_{RL,i} = \sin\phi_{rec,i} |\mathbf{I}_{rx,i}|, \quad (10)$$

where

$$\phi_{rec,i} = \arctan \left[\frac{1 - \cos 2\pi D_i}{\sin(2\pi D_i) + 2\pi(1 - D_i)} \right]. \quad (11)$$

It is known that in the Class E rectifier the relationship among D_i , $R_{L,i}$ and $C_{r,i}$ is

$$\begin{aligned} C_{r,i} &= \frac{[\sin(2\pi D_i) + 2\pi(1 - D_i)]^2}{2\pi\omega(R_{L,i} + r_{L_f,i} + r_{D_r,i})[1 - \cos(2\pi D_i)]} \\ &+ \frac{1 - 2\pi^2(1 - D_i)^2 - \cos(2\pi D_i)}{2\pi\omega(R_{L,i} + r_{L_f,i} + r_{D_r,i})}, \end{aligned} \quad (12)$$

which is due to the relationship among average voltage across the diode $D_{r,i}$, rectifier dc output voltage, and dc voltage drop on the RF choke $L_{f,i}$, as derived in [3]. Thus the duty cycle D_i can be designed by choosing a proper shunt capacitor $C_{r,i}$. This $C_{r,i}$ will influence $\phi_{rec,i}$ and $R_{rec,i}$, and eventually $\mathbf{R}_{tr,i}$ [refer to (8)(11)].

From (6) and (10), the power received by the i -th load can be calculated as

$$P_{RL,i} = I_{RL,i}^2 R_{L,i} = (\sin\phi_{rec,i} |\mathbf{R}_{tr,i}| |\mathbf{I}_{tx}|)^2 R_{L,i}. \quad (13)$$

Again, $C_{r,i}$ can be properly designed to tune $\phi_{rec,i}$, $\mathbf{R}_{tr,i}$, and thus $P_{RL,i}$, namely the power distributed to a specific load in the multiple-receiver WPT system. With (6) and (13), the overall power transfer efficiency from the transmitting coil to the final loads, $\eta_{coil2load}$, can be calculated as in (14). It can be seen that the efficiency also relates to $C_{r,i}$. A design methodology is required to determine the values of $C_{r,i}$'s taking into account both the power distribution and efficiency at the same time, as discussed later in Section III-A.

$$\eta_{coil2load} = \frac{2 \sum_{i=1}^n (\sin \phi_{rec,i} |\mathbf{R}_{tr,i}|)^2 R_{L,i}}{r_{tx} + \sum_{i=1}^n |\mathbf{R}_{tr,i}|^2 (r_{rx,i} + R_{rec,i})}. \quad (14)$$

B. Performance Analysis

In this paper, a planar multiple-receiver WPT system is assumed, in which the coupling between the transmitting coil and each receiving coil, namely k_{ti} , is supposed to be fixed. Note that coil design has been intensively studied to achieve homogeneous coupling against different horizontal misalignments [16]–[18]. Meanwhile, the coupling (i.e., distance) between the receiving coils, namely, k_{ij} , could vary in real applications. But, in a limited wireless charging area such as over a charging mat, the variation range of k_{ij} 's is usually predictable according to the maximum/minimum distances between the receiving coils.

1) *Negligible cross coupling*: It is known that in the planar WPT systems the cross coupling between the receiving coils is negligible (i.e., $k_{ij} \approx 0$) when the distance between the two coils are sufficiently large. Assuming negligible cross coupling, (3) can be further simplified by letting all the M_{ij} 's be zero. $\mathbf{R}_{tr,i}$ with negligible cross coupling can then be derived as

$$\mathbf{R}_{tr,i} = \frac{\mathbf{I}_{rx,i}}{\mathbf{I}_{tx}} = -\frac{j\omega M_{ti}}{r_{rx,i} + R_{rec,i}}. \quad (15)$$

Substituting (15) into (13) gives (16).

$$P_{RL,i} = \left(\frac{\omega M_{ti} |\mathbf{I}_{tx}| \sin \phi_{rec,i}}{r_{rx,i} + R_{rec,i}} \right)^2 R_{L,i}, \quad (16)$$

in which a constant \mathbf{I}_{tx} can be provided by the CM Class E PA. M_{ti} is also fixed. As discussed above, both $\phi_{rec,i}$ and $R_{rec,i}$ are determined by the value of $C_{r,i}$. Thus with negligible cross coupling, a decoupled multiple-receiver WPT system can be achieved, in which the distributed power to each load is solely determined by the design of $C_{r,i}$. In principle, this decoupled load power distribution is straightforward with a constant PA output current. Meanwhile, in terms of implementation, there are new requirements for the circuit configuration, theoretical analysis, and parameter design, as discussed and developed in this paper.

A well-established radio frequency (RF) circuit simulation tool, Advanced Design System (ADS) from Keysight Technologies (formerly Agilent's Electronic Measurement), is used to investigate the relationships among $C_{r,i}$, $P_{RL,i}$, and $\eta_{coil2load}$. All the ADS-based simulation uses the Harmonic

Balance, which is suitable for high-frequency circuit and system simulation. Here the number (order) of harmonics is 27 in the simulation. Parameters of the example two-receiver WPT system (TX , RX_1 , and RX_2) are as same as those in the final experiments, as listed in Table I. $|\mathbf{I}_{tx}|$ is chosen as 1 A. The two receiving coils are assumed to be identical but with different final loads. The Spice model of diode DFSL260 is employed in the simulation. $P_{RL,i}$ and $\eta_{coil2load}$ are obtained by sweeping the design parameters, $C_{r,1}$ and $C_{r,2}$, from 50 pF to 2000 pF. The compensation capacitors, $C_{rx,1}$ and $C_{rx,2}$, are then tuned accordingly to enable resonance of the coils [refer to (2)].

Fig. 2 shows the simulation results. As expected, the distributed load power of a specific receiver is solely determined by the value of its corresponding $C_{r,i}$ [see Fig. 2(a)(b)]. It is worth noticing that the relationship between $P_{RL,i}$ and $C_{r,i}$ demonstrates a good linearity over a wide range of power level. Fig. 2(c) shows that $\eta_{coil2load}$ maintains above 81.5% over the sweeping ranges of $C_{r,1}$ and $C_{r,2}$. It reaches the peak value, 84.8%, when $C_{r,1}$ and $C_{r,2}$ are 289 pF and 400 pF, respectively. The yellow star in the three subfigures correspond to a set of design parameters, $C_{r,1}$ and $C_{r,2}$, to deliver target load power to each load, 10 W for $P_{RL,1}$ and 8 W for $P_{RL,2}$. However, this set of $C_{r,i}$'s does not necessarily enable the peak efficiency of $\eta_{coil2load}$. Note that the magnitude of transmitting coil current $|\mathbf{I}_{tx}|$ can also provide another degree of design freedom. In the following section, both $C_{r,i}$'s and $|\mathbf{I}_{tx}|$ are chosen as design parameters to simultaneously provide the target load powers and reach the highest possible $\eta_{coil2load}$.

2) *With cross coupling*: Fig. 3 shows $P_{RL,1}$, $P_{RL,2}$, and $\eta_{coil2load}$ versus $C_{r,1}$ and $C_{r,2}$ when k_{12} is assumed to be strong, 0.04362 (46.3% of k_{ti}). This value of k_{12} corresponds to the strongest cross coupling in the following final experiments. Comparing with Fig. 2, Fig. 3 shows that when the cross coupling is strong the power distribution in the high power region is especially affected, while in the low power region the power distribution is still close to that of the case with negligible cross coupling. At the same time, high $\eta_{coil2load}$ is observed in both cases. As shown in Fig. 3, the existence of cross coupling particularly influences the actual power distribution among the receivers. In the real applications of the multiple-receiver WPT systems, the presence and variation of the cross coupling (i.e., k_{ij} 's) are often unavoidable due to changes in relative positions of the receivers. Thus, it is important to develop a design methodology that takes into account both desired load power distribution and system efficiency assuming varying k_{ij} 's, as discussed in the below section.

III. DESIGN METHODOLOGY

A. Parameter Design

As discussed above, $|\mathbf{I}_{tx}|$ and $C_{r,i}$'s are chosen as design parameters,

$$\mathbf{x} = [|\mathbf{I}_{tx}|, C_{r,1}, C_{r,2}, \dots, C_{r,n}]_{1 \times (1+n)}, \quad (17)$$

with a feasible range of

$$\mathbf{x} \in (\mathbf{x}^{\text{low}}, \mathbf{x}^{\text{upp}}), \quad (18)$$

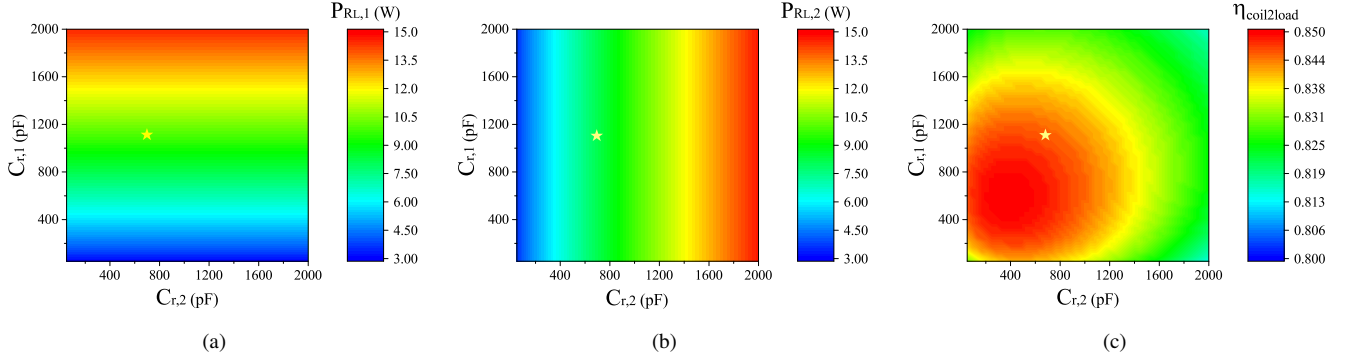


Fig. 2. Distributed load powers ($P_{RL,1}$ and $P_{RL,2}$) and system efficiency ($\eta_{coil2load}$) versus shunt capacitor capacitances ($C_{r,1}$ and $C_{r,2}$) with negligible cross coupling. (a) $P_{RL,1}$. (b) $P_{RL,2}$. (c) $\eta_{coil2load}$.

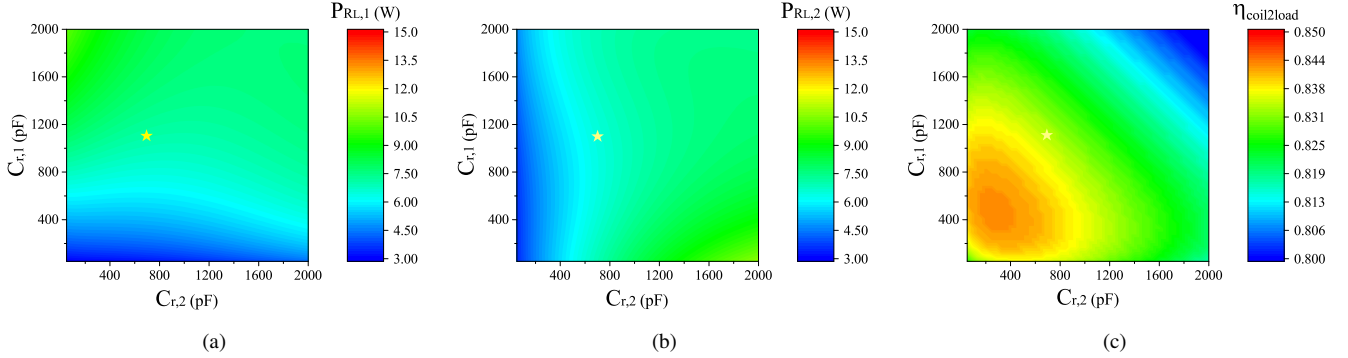


Fig. 3. Distributed load powers ($P_{RL,1}$ and $P_{RL,2}$) and system efficiency ($\eta_{coil2load}$) versus shunt capacitor capacitances ($C_{r,1}$ and $C_{r,2}$) with strong cross coupling ($k_{12}=0.04362$). (a) $P_{RL,1}$. (b) $P_{RL,2}$. (c) $\eta_{coil2load}$.

where \mathbf{x}^{low} and \mathbf{x}^{upp} are the lower and upper bounds of \mathbf{x} , respectively. The below parameters are treated as constant parameters, \mathbf{p} , which are supposed to be pre-determined during the initial design.

$$\mathbf{p} = [\omega, L_{tx}, r_{tx}, \mathbf{p}_1, \mathbf{p}_2, \dots, \mathbf{p}_n]_{1 \times (3+6n)}, \quad (19)$$

where

$$\mathbf{p}_i = [k_{ti}, L_{rx,i}, r_{rx,i}, r_{L,i}, r_{D_r,i}, R_{L,i}]_{1 \times 6}. \quad (20)$$

For a n -receiver WPT system, the number of possible combinations of any two receiving coils is

$$C_n^2 = \frac{n!}{2(n-2)!}. \quad (21)$$

Thus the array of the mutual inductance coefficients between any two receiving coils (i.e., the cross coupling) becomes

$$\mathbf{k} = [k_{12}, k_{13}, \dots, k_{ij}, \dots, k_{(n-1)n}]_{1 \times C_n^2}, \quad (22)$$

with the predicated variation range of

$$\mathbf{k} \in (\mathbf{k}^{\text{low}}, \mathbf{k}^{\text{upp}}). \quad (23)$$

Again \mathbf{k}^{low} and \mathbf{k}^{upp} are both $1 \times C_n^2$ vectors denoting the lower and upper bounds of \mathbf{k} . Then the efficiency from the transmitting coil to final dc loads, $\eta_{coil2load}$, can be expressed as follows [refer to (14)],

$$\eta_{coil2load,m}(\mathbf{x}, \mathbf{k}) = f_m(\mathbf{x}, \mathbf{p}, \mathbf{k}), \quad m \in (1, 2^n - 1). \quad (24)$$

The subscript m is an integer from 1 to $2^n - 1$. It corresponds to all the possible combinations of the receivers because

$$C_n^1 + C_n^2 + \dots + C_n^n = 2^n - 1. \quad (25)$$

The distributed dc load powers can also be expressed as a function of \mathbf{x} , \mathbf{p} , and \mathbf{k} [refer to (13)],

$$P_{RL,i,m}(\mathbf{x}, \mathbf{k}) = h_{i,m}(\mathbf{x}, \mathbf{p}, \mathbf{k}), \quad i \in (1, n) \text{ and } m \in (1, 2^n - 1). \quad (26)$$

Here i refers to the i -th receiver. In order to quantify the influences of the cross coupling, the below two indices, $\chi(\mathbf{x})$ and $\gamma(\mathbf{x})$, are defined to describe the deterioration in the efficiency and power distribution, respectively.

$$\chi(\mathbf{x}) = \max_{\mathbf{x}} \left| \frac{\eta_{coil2load,m}(\mathbf{x}, \mathbf{k}) - \eta_{coil2load,m}(\mathbf{x}, \mathbf{k}=\mathbf{0})}{\eta_{coil2load,m}(\mathbf{x}, \mathbf{k}=\mathbf{0})} \right|, \quad (27)$$

and

$$\gamma(\mathbf{x}) = \max_{\mathbf{x}} \left| \frac{P_{RL,i,m}(\mathbf{x}, \mathbf{k}) - P_{RL,i}^*}{P_{RL,i}^*} \right|, \quad (28)$$

with

$$\mathbf{k} \in (\mathbf{k}^{\text{low}}, \mathbf{k}^{\text{upp}}), \quad i \in (1, n), \text{ and } m \in (1, 2^n - 1). \quad (29)$$

$P_{RL,i}^*$ is the target load power of the i -th receiver. Smaller $\chi(\mathbf{x})$ and $\gamma(\mathbf{x})$ correspond to enhanced robustness in power distribution and efficiency against variation in the cross coupling, and vice versa. In the below optimization problem, (30), $\eta_{coil2load}$ under the target nominal condition (i.e., with

all the n receivers and negligible cross coupling) is chosen as the objective function, namely maximizing $\eta_{coil2load}^{nom}(\mathbf{x})$. χ^{\max} and γ^{\max} in the two constraints are added to restrict the variation ranges of $\chi(\mathbf{x})$ and $\gamma(\mathbf{x})$, and thus guarantee proper robustness of the system performance when cross coupling between the receiving coils happens.

$$\begin{aligned} \max_{\mathbf{x}} \quad & \eta_{coil2load}^{nom}(\mathbf{x}), \\ \text{s.t.} \quad & \chi(\mathbf{x}) \leq \chi^{\max}, \\ & \gamma(\mathbf{x}) \leq \gamma^{\max}. \end{aligned} \quad (30)$$

Given the nature of the above nonlinear optimization problem, genetic algorithm (GA), a popular population-based heuristic approach, is an effective tool to search the global or at least close-to-global optimal solution [19], [20].

B. Current-Mode PA Design

A constant current is preferred to drive the transmitting coil enabling a multiple-receiver WPT system to operate with a scalable number of receivers. However, the classical Class E PA is well known for its high sensitivity in loading conditions. As shown Fig. 1(a), a current-mode (CM) Class E PA is designed with an additional Π impedance transformation network. If the variation range of the PA load, \mathbf{Z}_{coil} here, is predictable, a high efficiency and constant output current Class E PA, i.e., an initial design goal, can be achieved by designing the impedance transformation network via the load-pull simulation [21]. The target of the network design is to determine the values of L_{mn} , C_{ml} , and C_{mr} that match the load-variation line of \mathbf{Z}_{mn} (i.e., load of the classical Class E PA in Fig. 1(a)) as closely as possible to a reference line in the Smith chart. This reference line should be selected to be in the high efficiency region and only intersect each power contour once to maintain high efficiency and monotonicity of output power when \mathbf{Z}_{coil} changes, namely a characteristic of the CM PA [see Fig. 5]. As mentioned in detail in Ref. [21], a design optimization problem can be formulated to solve the parameters of the Π impedance transformation network. Other networks, such as L and T ones, can also be designed and compared to determine the best topology, i.e., Π network here, in terms of matching performance and network insertion loss. A recent reference, Ref. [22], designs a load-independent Class EF inverter that acts as a current source under a varying load resistance. A different approach from [21] is adopted to achieve the current source inverter by using the Π impedance transformation network and load-pull simulation technique. This approach can also be used for different inverter topologies to improve their load conditions, such as CM Class D and Class E inverters. Similarly, the proposed system-level design approach can be extended to multiple-receiver WPT systems with other inverter and rectifier topologies.

In this paper, this design is further extended for the present application with a scalable number of receivers. From (3), the load seen by the CM Class E PA, \mathbf{Z}_{coil} , can be derived as

$$\mathbf{Z}_{coil} = \frac{\mathbf{V}_{tx}}{\mathbf{I}_{tx}} = r_{tx} + \sum_{i=1}^n j\omega M_{ti} \mathbf{R}_{tr,i}. \quad (31)$$

With negligible cross coupling, substituting (15) into (31) gives

$$\mathbf{Z}_{coil} = r_{tx} + \sum_{i=1}^n \frac{\omega^2 M_{ti}^2}{r_{rx,i} + R_{rec,i}}. \quad (32)$$

The above \mathbf{Z}_{coil} in (32) is obviously pure resistive. Thus the design of the CM Class E PA simply follows the same design procedure in [21]. However, with the cross coupling, the extra reactance component of \mathbf{Z}_{coil} in (31) makes the design of the PA challenging. Note that in the present multiple-receiver WPT system, the variation of the PA load (\mathbf{Z}_{coil}) is mostly caused by adding or removing receivers. Naturally, the maximum \mathbf{Z}_{coil} occurs when all the n receivers involve, and the minimum \mathbf{Z}_{coil} happens when there is only one receiver with the lowest required power. \mathbf{Z}_{coil}^{low} ($=R_{coil}^{low}$) is pure resistive because the cross coupling is negligible, while \mathbf{Z}_{coil}^{upp} is a complex impedance. An intermediate R_{coil}^* , i.e., in terms of the real part, could be chosen as a nominal load for the classical Class E PA itself, namely

$$R_{coil}^* = \frac{R_{coil}^{low} + Re\{\mathbf{Z}_{coil}^{upp}\}}{2}. \quad (33)$$

$Re\{*\}$ means the real part of a complex number. Thus the parameters of classical Class E PA, i.e., C_S , and C_0 , can be determined following the below equations [23],

$$C_S = \frac{0.1836}{\omega R_{coil}^*}, \quad (34)$$

$$C_0 = \frac{1}{\omega^2 L_0 - 1.1525\omega R_{coil}^*}. \quad (35)$$

Based on the designed classical Class E PA, the values of C_{ml} , C_{mr} , and L_{mn} , i.e., the added impedance transformation network, can be determined by the load-pull simulation, as explained in detail in Section IV-A. Note that theoretically the circuit topology of the CM Class E PA could be further simplified, such as using the Π network to not only perform the impedance transformation but also to compensate the transmitting coil and provide a proper residual inductance required from the PA. At the same time, from a practical point of view, the series connected LC network (L_0 and C_0 in Fig. 1(a)) not only provides the residual inductance, but also acts as a band pass filter to help reduce harmonic content and suppress distortion of the PA waveform. A different design is also possible to have a Class E PA with a low quality-factor series LC network.

IV. EXPERIMENTAL VERIFICATION

An example 6.78-MHz WPT system is built up with maximum three receivers included at the same time. As shown in Fig. 4, the below large coil is the transmitting coil, and the upper three distributed small coils are the receiving coils. This experimental system shares the same circuit configuration with the one in Fig. 1. It aims to deliver 10 W, 8 W, 6 W powers to 10 Ω , 8 Ω , 12 Ω loads, respectively. Electronic loads are employed to emulate the final dc loads and measure the output powers. The air gap between the transmitting coil and receiving coils is 22 mm. 150-V MOSFET SUD15N15 is used in the CM Class E PA, and 60-V Schottky diodes DFSL260

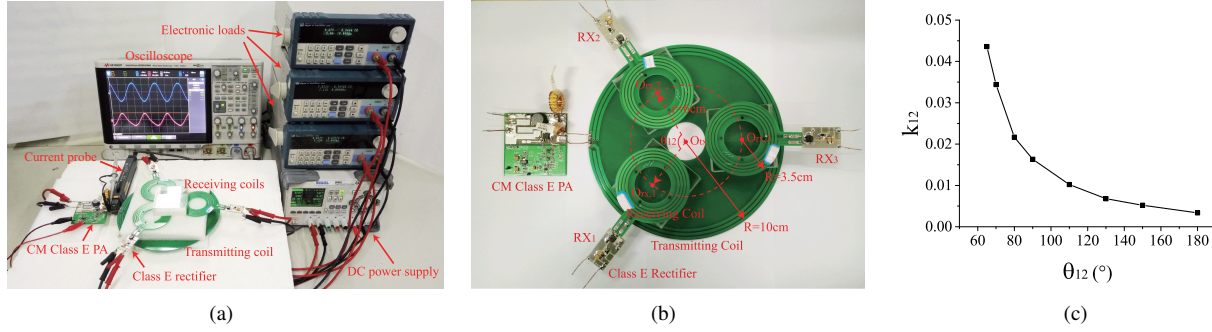


Fig. 4. Experimental multiple-receiver WPT system. (a) Overall system. (b) Layout of coils. (c) k_{12} versus θ_{12} .

are used in the three Class E rectifiers. All the constant parameters and target load powers of the three receivers are listed in Table I. Again, C_{tx} is designed to fully resonant with L_{tx} [refer to (1)].

As shown in Fig. 4(b), for the sake of simplicity, the three receiving coils are all with the same size. In the experiments, they are moved along a circle (i.e., red dashed line) with the same center of the transmitting coil, and a radius of 6 cm. This guarantees the same and fixed mutual inductance coefficients, $k_{ti}=0.09414$, between each receiving coil and the transmitting coil. Fig. 4(c) shows the measured k_{12} (i.e., the cross coupling between RX_1 and RX_2) versus θ_{12} in Fig. 4(b) by moving one of the RX along the red dashed circle. It is obvious that when the θ_{12} is 180° , the receiving coils are most loosely coupled ($k_{12}=0.00338$), and when the angular separation is 65° (the receiving coils are adjacent to each other), the two receiving coils become strongly coupled ($k_{12}=0.04362$). The mutual inductances between the coils (i.e., M_{ti} and M_{ij}) can be calculated based on the measured mutual inductance coefficients [refer to (4)(5)]. In the experiments, M_{ij} varies between $0.004975 \mu\text{H}$ and $0.06421 \mu\text{H}$, while M_{ti} is fixed at $0.2347 \mu\text{H}$, i.e. a planar WPT system.

TABLE I
PARAMETERS IN EXPERIMENTAL SYSTEM ($i=1,2,3$)

ω	6.78 MHz	C_{tx}	131 pF
L_{tx}	4.221 μH	r_{tx}	1.1 Ω
$L_{rx,i}$	1.472 μH	$r_{rx,i}$	0.3 Ω
$R_{L,1}$	10 Ω	k_{ti}	0.09414
$R_{L,2}$	8 Ω	$L_{f,i}$	10 μH
$R_{L,3}$	12 Ω	$r_{L_{f,i}}$	0.1 Ω
$P_{R_{L,1}}^{tar}$	10 W	$r_{D_{r,i}}$	0.4 Ω
$P_{R_{L,2}}^{tar}$	8 W	C_o	32 μF
$P_{R_{L,3}}^{tar}$	6 W	-	-

A. Parameter Design

Based on the design procedure developed in Section III-A, the feasible ranges of the design parameters, \mathbf{x}^{upp} and \mathbf{x}^{low} , should be first specified, which should be sufficiently large and thus provide required design freedom. Here the feasible

range of $|\mathbf{I}_{tx}|$ is finalized as (0.3 A, 3 A) and feasible range of $C_{r,i}$ is chosen as (50 pF, 2000 pF), namely

$$\mathbf{x}^{\text{low}} = [0.3 \text{ A}, 50 \text{ pF}, 50 \text{ pF}, 50 \text{ pF}], \quad (36)$$

$$\mathbf{x}^{\text{upp}} = [3 \text{ A}, 2000 \text{ pF}, 2000 \text{ pF}, 2000 \text{ pF}]. \quad (37)$$

The variation range of the mutual inductance coefficients between the receiving coils, i.e., the cross coupling, is determined based on the actual measurements,

$$\mathbf{k}^{\text{low}} = [0.00338, 0.00338, 0.00338], \quad (38)$$

$$\mathbf{k}^{\text{upp}} = [0.04362, 0.04362, 0.04362]. \quad (39)$$

The vector \mathbf{k} includes three elements, k_{12} , k_{13} , k_{23} . \mathbf{k}^{low} and \mathbf{k}^{upp} are chosen according to the cases of $\theta_{ij}=180^\circ$ and 65° , respectively, as illustrated in Fig. 4(c). The indexes, χ^{max} and γ^{max} , are both specified as 0.1. Note that a too small index requires high robustness, and thus may lead to poor efficiency or no convergence of solution of the optimization problem, while a large index sacrifices the robustness against the variation in the cross coupling.

Finally, the optimal set of design parameters for the experimental multiple-receiver WPT system is finalized following the design procedure in Section III-A,

$$[|\mathbf{I}_{tx}|, C_{r,1}, C_{r,2}, C_{r,3}] = [1.28 \text{ A}, 628 \text{ pF}, 303 \text{ pF}, 220 \text{ pF}]. \quad (40)$$

The compensation capacitors of the receiving coils, $C_{rx,i}$, are then determined to achieve full resonance on the receiving side considering the non-zero input reactances of the Class E rectifiers [refer to (2)],

$$[C_{rx,1}, C_{rx,2}, C_{rx,3}] = [423 \text{ pF}, 423 \text{ pF}, 447 \text{ pF}]. \quad (41)$$

Note that the above final capacitances in (40)(41) are determined after also considering products available on the market. With the above results, the variation range of the input impedance of the transmitting coil, \mathbf{Z}_{coil} , can be determined accordingly that guides the design of the CM Class E PA. Based on (31), the values of \mathbf{Z}_{coil} under the seven possible combinations of the three receiving coils (RXs) are firstly calculated assuming the maximum $k_{ij}(=0.04362)$. The results are summarized in Table II.

Thus the variation range of \mathbf{Z}_{coil} is

$$\mathbf{Z}_{\text{coil}} \in (10.10 \Omega, 26.97 - j18.58 \Omega). \quad (42)$$

TABLE II
 \mathbf{Z}_{coil} UNDER VARIOUS RX COMBINATIONS.

1 RX	RX_1	RX_2	RX_3
$\mathbf{Z}_{\text{coil}} (\Omega)$	15.79	13.44	10.10
2 RXs	$RX_{1,2}$	$RX_{1,3}$	$RX_{2,3}$
$\mathbf{Z}_{\text{coil}} (\Omega)$	24.90-j8.74	23.47-j6.91	20.80-j5.61
3 RXs	$RX_{1,2,3}$	-	-
$\mathbf{Z}_{\text{coil}} (\Omega)$	26.97-j18.58	-	-

Similarly, the variation range of \mathbf{Z}_{coil} with the minimum k_{ij} (=0.00338) can be also determined as

$$\mathbf{Z}_{\text{coil}} \in (10.10 \Omega, 37.04 - j1.80 \Omega). \quad (43)$$

As discussed in Section III-B, an intermediate pure-resistive load, 20 Ω , is chosen to calculate C_S and C_0 in the classical Class E PA [refer to (34) and (35)]. Then with the variation ranges of \mathbf{Z}_{coil} , the parameters of the impedance transformation network, C_{ml} , L_{mn} , and C_{mr} , can be determined through the load-pull simulation. Final parameters of the CM Class E PA are listed in Table III.

TABLE III
PARAMETERS OF CM CLASS E PA.

V_{dc}	L_Q	C_S	L_0
32 V	68 μH	215 pF	1.404 μH
C_0	L_{mn}	C_{ml}	C_{mr}
642 pF	414 nH	330 pF	490 pF

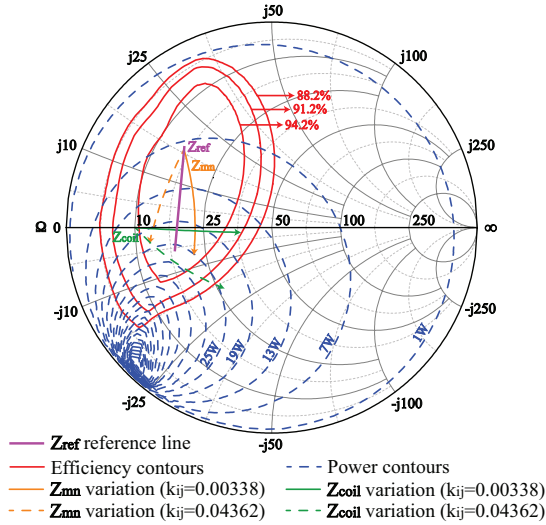


Fig. 5. Load-pull simulation results.

The load-pull simulation results are shown in the Smith chart in Fig. 5. The purple solid line is the reference line, \mathbf{Z}_{ref} . As discussed in Section III-B, it is defined as a reference impedance trajectory that is within the high-efficiency region and only intersects each power contour once. This reference trajectory provides guidance for the following design of the impedance transformation network. The red solid lines

and blue dashed lines are the efficiency and output power contours of the classical Class E PA under different PA loads, respectively. The green and orange lines show the trajectories of variation in the PA load with the minimum and maximum k_{ij} [refer to (42) and (43)]. Note that \mathbf{Z}_{coil} is the load of the classical Class E PA, namely without the newly added impedance transformation network, while \mathbf{Z}_{mn} is the improved PA load after the impedance transformation, i.e., the load of the CM Class E PA. The network is accordingly designed, as discussed in section III-B. Both trajectories of \mathbf{Z}_{mn} with maximum and minimum cross coupling are well within the high PA efficiency region, above 94.2%. The trajectories move from low power region to high power region when \mathbf{Z}_{mn} increases, i.e., higher PA output power with an increasing load. These results validate the design of the high efficiency CM Class E PA when the cross coupling happens. Note that the trajectories of \mathbf{Z}_{mn} show that, thanks to the designed Π impedance transformation network, the residual inductance of the classical Class E PA is still dependant on the load, but with improved PA efficiency and output characteristics. The three-receiver WPT system in Fig. 4 is used as an example for validation purposes. A case with more receivers would mainly influence the operation of the CM Class E PA and thus adversely affect efficiency and the target power distribution. The above CM Class E PA is designed based on the load-pull simulation. As shown in Fig. 5, in order to maintain a high PA efficiency, the variation range of the PA load, i.e., \mathbf{Z}_{mn} , need to lie within the high efficiency region. Therefore, when the total number of the receivers is larger than its target number (e.g., three here), the PA load may possibly move beyond the high efficiency region in Fig. 5, and thus leads to a low PA efficiency. Similarly, the variation in PA load due to more receivers may also affect the PA output current. Meanwhile, the design methodology itself developed in section III is generic, allowing for more receivers. Note that, in addition to the above results of the load-pull simulation, \mathbf{Z}_{mn} can also be analytically derived based on \mathbf{Z}_{coil} to double check effectiveness of the designed Π network [see Fig. 1(a)] [21].

$$\mathbf{Z}_{\text{mn}} = \frac{jX_3(X_1 + X_2)\mathbf{Z}_{\text{coil}} - X_1X_2X_3}{(X_1 + X_2 + X_3)\mathbf{Z}_{\text{coil}} + jX_1(X_2 + X_3)}, \quad (44)$$

where

$$X_1 = -\frac{1}{\omega C_{mr}}, \quad X_2 = \omega L_{mn}, \quad X_3 = -\frac{1}{\omega C_{ml}}. \quad (45)$$

B. Experimental Results

In the present multiple-receiver WPT system, the target 1.28 A $|\mathbf{I}_{\text{tx}}|$ in (40) corresponds to 32.5 V V_{dc} , the PA input dc voltage [see Fig. 1]. Fig. 6 shows the load powers $P_{RL,i}$ versus $|\mathbf{I}_{\text{tx}}|$ when the three receivers are placed with 120° angular difference in positions. When $|\mathbf{I}_{\text{tx}}|$ is 1.28 A, the three loads receive their target powers, 9.60 W, 7.70 W, 5.81 W, respectively. High efficiency from the transmitting coil to the final loads, $\eta_{\text{coil2load}}$, is observed, about 86.2% in Fig. 6(b). The above efficiency is calculated based on the voltage and current measurements. To accurately measure the input power of the transmitting coil, the voltage probe and

current probe were calibrated to minimize their propagation delay difference at 6.78 MHz, using a 50-Ω non-inductive resistor. The calculation (cal.) and experimental (exp.) results match each well and thus validate the correctness of the above analytical derivations. The experimental $\eta_{coil2load}$ becomes slightly higher when $|\mathbf{I}_{tx}|$ increases because of the reduced ESR of the rectifying diodes at a higher power level.

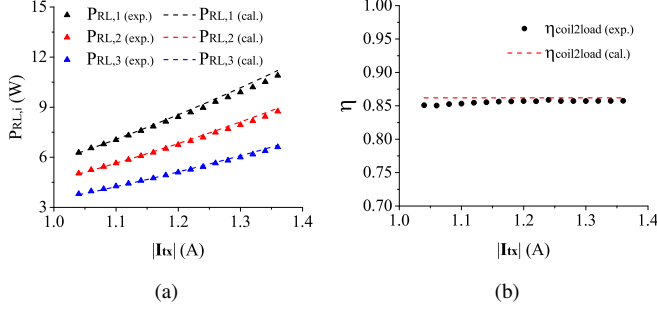


Fig. 6. Load powers and efficiency versus $|\mathbf{I}_{tx}|$. (a) $P_{RL,i}$. (b) $\eta_{coil2load}$.

The results in Fig. 8 validates the scalability of the multiple-receiver WPT system. The three receivers are first placed with 120° position difference. Then, during the following 700 s, after each 100 s, one of the receivers is removed, and returned later to the same position. The variations of the received load powers from their target values are significantly suppressed. The maximum errors for $P_{RL,1}$, $P_{RL,2}$ and $P_{RL,3}$ are 3.99%, 3.38%, 3.24%, respectively. The operation of the CM Class E PA is also investigated. The drain-source voltage V_{DS} and output current I_{tx} are shown in Fig. 7 under the various combinations of the receivers, where “No load” is the case without any receiver. The waveforms show that, within the target variation range of the PA load, the CM Class E PA largely keeps its soft-switching operation (i.e., zero-voltage-switching here) and almost constant output current, thanks to the designed Π impedance transformation network. The changing peak voltages are mostly due to the variation in \mathbf{Z}_{mn} , namely the load of the classical Class E PA [see the trajectories of \mathbf{Z}_{mn} in Fig. 5].

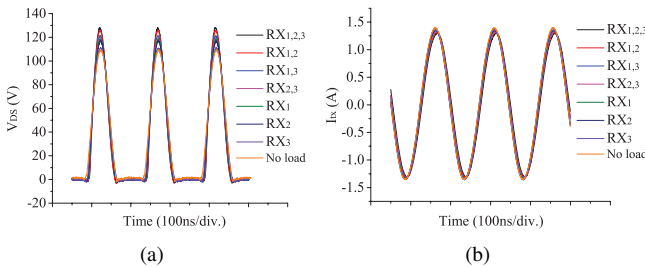


Fig. 7. Waveforms of the CM Class E PA under different combinations of receivers. (a) Drain-source voltage V_{DS} . (b) Output current I_{tx} .

As summarized in Table IV, both the system efficiency and PA efficiency maintain a high value, above 70% and 89%, respectively, in all the seven combinations. For reference purposes, the results of other two cases are also co-listed in Fig. 8. These two cases are

- 1) “no optimization”: the conventional design explained in Section II-B1 is applied with the 1 A $|\mathbf{I}_{tx}|$. It assumes negligible cross coupling [see $P'_{RL,1-3}$].
- 2) “rectifier optimization only”: the impedance transformation network designed through the load-pull simulation is removed from the CM Class E PA [see $P''_{RL,1-3}$]. Therefore, the PA is simply a classical Class E PA. All the other parameters are as same as those in the proposed design.

As shown in Fig. 8, both the above two cases obviously fail to maintain the target power demand of each receiver when the number of receivers varies over time.

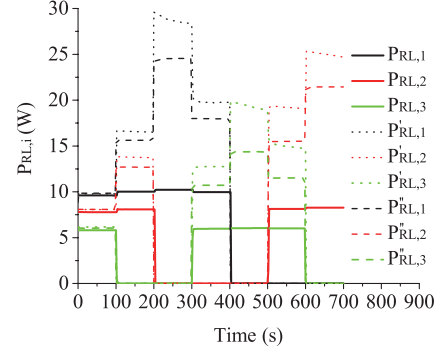


Fig. 8. Load powers under different combinations of receivers.

TABLE IV
EFFICIENCIES UNDER DIFFERENT COMBINATIONS OF RECEIVERS.

1 RX	RX_1	RX_2	RX_3
η_{pa}	90.87%	90.39%	89.18%
η_{sys}	73.99%	71.68%	70.82%
2 RXs	$RX_{1,2}$	$RX_{1,3}$	$RX_{2,3}$
η_{pa}	91.94%	92.11%	91.85%
η_{sys}	77.46%	77.88%	77.69%
3 RXs	$RX_{1,2,3}$	-	-
η_{pa}	91.91%	-	-
η_{sys}	78.43%	-	-

In order to investigate the performance when the cross coupling exists, the two receivers, RX_1 and RX_2 , are first placed with $\theta_{12}=180^\circ$, i.e., a two-receiver system. RX_1 is moved later along the dashed-line circle in Fig. 4(b). The delivered load powers, $P_{RL,1}$ and $P_{RL,2}$, are measured versus the changing θ_{12} , and the PA dc input voltage V_{dc} is fixed at 32.5 V. As shown in Fig. 9(a), the target power distribution is well preserved over wide range of θ_{12} from 180° to 100° . As the cross coupling becomes stronger, the load power $P_{RL,1}$ and $P_{RL,2}$ firstly increase and then decrease. This is due to the slight variation of $|\mathbf{I}_{tx}|$ caused by the cross coupling. The maximum error in $P_{RL,1}$ and $P_{RL,2}$ is small, 1.8% and 4.4%, respectively. High system efficiency η_{sys} (above 77%) and $\eta_{coil2load}$ are also observed, as shown in Fig. 9(b). Again, the results of the other two cases are co-listed in Fig. 9. $P'_{RL,1-2}$, η'_{sys} , and $\eta'_{coil2load}$ are for “no optimization” case; and $P''_{RL,1-2}$, η''_{sys} , and $\eta''_{coil2load}$ are for “rectifier

optimization only” case. The proposed design demonstrates obviously improved performance in load power distribution when comparing with the two reference cases [see Fig. 9(a)]. It is interesting to note that in Fig. 9(b) η_{sys} is higher than η_{sys} , even though the “rectifier optimization only” case does not employ the impedance transformation network, a component bringing an additional power loss. This result further validates performance improvement of the CM Class *E* PA through the load-pull simulation, not only in terms of load power distribution but for efficiency.

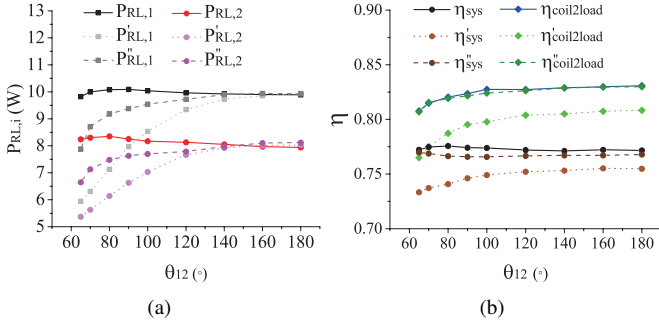


Fig. 9. Load powers and efficiencies. (a) Load powers. (b) Efficiencies.

For reference purposes, the loss breakdown of the entire system is listed in Table V, taking the case of three receivers (120° position difference) as an example. “Rec_{rx,i}” denotes the rectifier of the *i*-th receiver. The power loss in the PA is measured according to its input dc power and output ac power. Similarly, the power losses in the rectifiers are measured based on their input ac powers and output dc powers. The measured currents of the transmitting coil and three receiving coils are used to calculate the power losses in the coupling coils using their parasitic parameters. The PA driving loss can be directly read from the power supply. Note that in the above discussions, the PA driving loss is neglected because it is comparatively small and almost constant. The maximum power loss on the MOSFET of the CM Class *E* PA, *Q* in Fig. 1(a), is about 1.4 W. Thermal image of the PA at its maximum output power is given in Fig. 10. The highest temperature of the MOSFET is about 55.3 °C, and the temperatures of the three inductors, *L_Q*, *L₀* and *L_{mn}*, are all below 50 °C. Note that no heat sink or fan is used.

TABLE V
LOSS BREAKDOWN WITH THREE RECEIVERS (W).

Rec _{rx,1}	Rec _{rx,2}	Rec _{rx,3}
0.76	0.73	0.45
Coil _{rx,1}	Coil _{rx,2}	Coil _{rx,3}
0.52	0.35	0.17
Coil _{tx}	CM PA	PA Driving
1.00	2.53	0.38

Finally, in real applications, the final load, i.e., $R_{L,i}$ here, may change depending on its required power. First, the proposed design avoids interference among the received powers when such a case happens, as shown in Fig. 11 taking

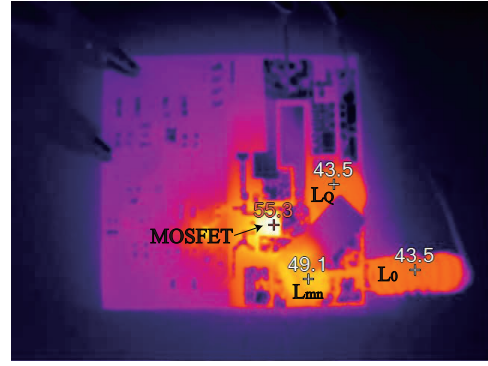


Fig. 10. Thermal image of the CM Class *E* PA at its maximum output power.

changing $R_{L,1}$ as an example. Second, if the load requires a voltage regulator on the receiving side, the proposed design also reduces the required voltage tuning range due to the pre-designed target power distribution. This helps improve efficiency and lower the required voltage operating range of the regulator.

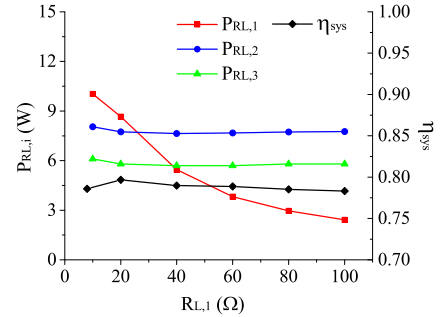


Fig. 11. An example of interference avoidance when $R_{L,1}$ changes – load power ($P_{R_{L,i}}$) and system efficiency (η_{sys}) versus $R_{L,1}$.

V. CONCLUSIONS

This paper develops a systematic circuit design methodology for high-efficiency WPT systems with a scalable number of receivers. The shunt capacitor in the Class *E* rectifiers is particularly chosen as a design parameter to tune the input impedance of the rectifiers. Further combining with the constant PA output current (i.e., another design parameter), a target load power for a specific receiver can be naturally delivered and maintained. An impedance transformation network is added to the classical Class *E* PA. This network is designed later to enable an almost constant PA output current over a specific variation range of the PA load caused by the changing receiver number and cross coupling. A design optimization problem is then formulated and solved to determine the design parameters that provide robustness of the system performance, again, under variations in receiver number and cross coupling. Both the simulation and experimental results validate the correctness of the analytical derivations and parameter design. The proposed solution combines efforts in circuit topology, modeling, high-fidelity simulation, and design optimization. It

enables the concise circuit configuration of the final multiple-receiver WPT system.

REFERENCES

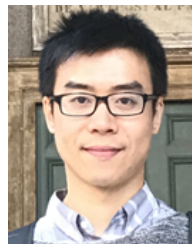
- [1] S. Aldhafer, D. C. Yates, and P. D. Mitcheson, "Design and development of a Class EF₂ inverter and rectifier for multimegahertz wireless power transfer systems," *IEEE Trans. on Power Electron.*, vol. 31, no. 12, pp. 8138–8150, Dec. 2016.
- [2] E. Ozalevli, N. Femia, G. D. Capua, R. Subramonian, D. Du, J. Sankman, and M. E. Markhi, "A cost-effective adaptive rectifier for low power loosely coupled wireless power transfer systems," *IEEE Trans. Circuits Syst. I*, 2017, DOI:10.1109/TCSI.2017.2780169.
- [3] M. Liu, M. Fu, and C. Ma, "Parameter design for a 6.78-MHz wireless power transfer system based on analytical derivation of Class E current-driven rectifier," *IEEE Trans. Power Electron.*, vol. 31, no. 6, pp. 4280–4291, Jun. 2016.
- [4] Y. Yang, W. Zhong, S. Kiratipongvoot, S. C. Tan, and S. Y. R. Hui, "Dynamic improvement of series-series compensated wireless power transfer systems using discrete sliding mode control," *IEEE Trans. on Power Electron.*, vol. 33, no. 7, pp. 6351–6360, Jul. 2018.
- [5] F. Liu, Y. Yang, Z. Ding, X. Chen, and R. M. Kennel, "A multifrequency superposition methodology to achieve high efficiency and targeted power distribution for a multiloop MCR WPT system," *IEEE Trans. Power Electron.*, vol. 33, no. 10, pp. 9005–9016, Oct. 2018.
- [6] W. Zhong and S. Y. R. Hui, "Auxiliary circuits for power flow control in multifrequency wireless power transfer systems with multiple receivers," *IEEE Trans. Power Electron.*, vol. 30, no. 10, pp. 5902–5910, Oct. 2015.
- [7] "Wireless power transmission using technologies other than radio frequency beam," in *Document Report ITU-R SM.2303-2, Radiocommunication Sector, International Telecommunication Union*, Jun. 2017.
- [8] M. Fu, H. Yin, and C. Ma, "Megahertz multiple-receiver wireless power transfer systems with power flow management and maximum efficiency point tracking," *IEEE Trans. Microw. Theory Techn.*, vol. 65, no. 11, pp. 4285–4293, Nov. 2017.
- [9] Y. J. Kim, D. Ha, W. J. Chappell, and P. P. Irazoqui, "Selective wireless power transfer for smart power distribution in a miniature-sized multiple-receiver system," *IEEE Trans. on Ind. Electron.*, vol. 63, no. 3, pp. 1853–1862, Mar. 2016.
- [10] W. Wang, X. Huang, J. Guo, H. Liu, C. Yan, and L. Tan, "Power stabilization based on efficiency optimization for WPT systems with single relay by frequency configuration and distribution design of receivers," *IEEE Trans. Power Electron.*, vol. 32, no. 9, pp. 7011–7024, Sep. 2017.
- [11] H. Yin, M. Fu, M. Liu, J. Song, and C. Ma, "Autonomous power control in a reconfigurable 6.78-MHz multiple-receiver wireless charging system," *IEEE Trans. on Ind. Electron.*, vol. 65, no. 8, pp. 6177–6187, Aug. 2018.
- [12] M. Fu, T. Zhang, X. Zhu, P. C. K. Luk, and C. Ma, "Compensation of cross coupling in multiple-receiver wireless power transfer systems," *IEEE Trans. Ind. Informat.*, vol. 12, no. 2, pp. 474–482, Apr. 2016.
- [13] J. A. Santiago-Gonzalez, K. M. Elbaggari, K. K. Afridi, and D. J. Perreault, "Design of Class E resonant rectifiers and diode evaluation for VHF power conversion," *IEEE Trans. on Power Electron.*, vol. 30, no. 9, pp. 4960–4972, Sep. 2015.
- [14] M. K. Kazimierczuk, "Analysis of Class E zero-voltage-switching rectifier," *IEEE Trans. Circuits Syst.*, vol. 37, no. 6, pp. 747–755, Jun. 1990.
- [15] M. K. Kazimierczuk and D. Czarkowski, *Resonant Power Converters*, 2nd ed. NY, USA: John Wiley and Sons, 2011.
- [16] E. Waffenschmidt, "Homogeneous magnetic coupling for free positioning in an inductive wireless power system," *IEEE J. of Emerg. Sel. Topics in Power Electron.*, vol. 3, no. 1, pp. 226–233, Mar. 2015.
- [17] J. Kim, H. C. Son, and Y. J. Park, "Multi-loop coil supporting uniform mutual inductances for free-positioning WPT," *Electronics Letters*, vol. 49, no. 6, pp. 417–419, Mar. 2013.
- [18] S. Y. R. Hui and W. W. C. Ho, "A new generation of universal contactless battery charging platform for portable consumer electronic equipment," *IEEE Trans. Power Electron.*, vol. 20, no. 3, pp. 620–627, May 2005.
- [19] J. Bito, S. Jeong, and M. M. Tentzeris, "A novel heuristic passive and active matching circuit design method for wireless power transfer to moving objects," *IEEE Trans. Microw. Theory Techn.*, vol. 65, no. 4, pp. 1094–1102, Apr. 2017.
- [20] —, "A real-time electrically controlled active matching circuit utilizing genetic algorithms for wireless power transfer to biomedical implants," *IEEE Trans. Microw. Theory Techn.*, vol. 64, no. 2, pp. 365–374, Feb. 2016.

- [21] S. Liu, M. Liu, S. Yang, C. Ma, and X. Zhu, "A novel design methodology for high-efficiency current-mode and voltage-mode Class-E power amplifiers in wireless power transfer systems," *IEEE Trans. Power Electron.*, vol. 32, no. 6, pp. 4514–4523, Jun. 2017.
- [22] S. Aldhafer, D. C. Yates, and P. D. Mitcheson, "Load-independent Class E/EF inverters and rectifiers for MHz-switching applications," *IEEE Trans. on Power Electron.*, vol. 33, no. 10, pp. 8270–8287, Oct. 2018.
- [23] M. Albulet, *RF Power Amplifiers*. SciTech Publishing, 2001.



Jibin Song (S'16) received the B.S. degree in measurement and control technology and instrumentation with First Class Honors from Jilin University, Jilin, China, in 2016. He is currently working toward the Ph.D. degree in electrical and computer engineering with the University of Michigan-Shanghai Jiao Tong University Joint Institute, Shanghai Jiao Tong University, Shanghai, China.

His research interests include circuit-level and system-level designs of megahertz wireless power transfer systems, and circuit topologies and control strategies of high-frequency power electronics.



Ming Liu (S'15-M'17) received the B.S. degree in mechatronic engineering from Sichuan University, Sichuan, China, in 2007, and the Ph.D. degree in electrical and computer engineering from the University of Michigan-Shanghai Jiao Tong University Joint Institute, Shanghai Jiao Tong University, Shanghai, China, in 2017. He is currently a postdoctoral research fellow at Department of Electrical Engineering, Princeton University, Princeton, NJ, USA. His research interests include circuit topologies and architectures, control strategies, parameters design and optimization of megahertz wireless power transfer systems as well as high frequency power electronics.

Dr. Liu serves as Guest Editor of IEEE Transactions on Industrial Informatics and Chair of the Wireless Power Transfer for Energy Storage Charging Subcommittee of Energy Storage Technical Committee, IEEE Industrial Electronics Society. He received Top Ten Academic Star Award and Excellent PhD Thesis Award Nomination at Shanghai Jiao Tong University in 2016 and 2018, and Research Excellence Award from AirFuel Alliance, USA, in 2019.



Chengbin Ma (M'05-SM'18) received the B.S. degree in industrial automation from East China University of Science and Technology, Shanghai, China, in 1997, and the M.S. and Ph.D. degrees in electrical engineering from The University of Tokyo, Tokyo, Japan, in 2001 and 2004, respectively. From 2004 to 2006, he was an R&D Researcher with the Servo Motor Laboratory, FANUC Limited, Japan. Between 2006 and 2008, he was a Postdoctoral Researcher with the Department of Mechanical and Aeronautical Engineering, University of California, Davis, USA. He joined the University of Michigan-Shanghai Jiao Tong University Joint Institute, Shanghai Jiao Tong University, Shanghai, China, in 2008, and currently an Associate Professor of electrical and computer engineering. His research interests include energy management, megahertz wireless power transfer, dynamics and motion control, and wide applications in electronic devices, electric vehicles, microgrids, smart grids, etc.

Dr. Ma is an IEEE senior member. He serves as Delegate of Energy Cluster, Chair of Energy Storage Technical Committee and Chair of Shanghai Chapter, IEEE Industrial Electronics Society. He is an Associated Editor for the IEEE Transactions on Industrial Informatics. He won many teaching and research awards at Shanghai Jiao Tong University, such as Koguan Top Ten Best Teacher Award in 2017 and Koguan Top Ten Research Group Award in 2014. He also received Research Excellence Award from AirFuel Alliance, USA, in 2019.